Environmental Science and Pollution Research (2022) 29:222–235
https://doi.org/10.1007/s11356-021-15578-8

CYCLODEXTRIN APPLICATIONS IN PHARMACY, BIOLOGY, MEDICINE AND ENVIRONMENT

# Surface functionalization of natural hydroxyapatite by polymerization of β-cyclodextrin: application as electrode material for the electrochemical detection of Pb(II)

Rodrigue Tchoffo[1] · Guy B. P. Ngassa[1,2] · Giscard Doungmo[3] · Arnaud T. Kamdem[4] · Ignas K. Tonlé[1,5] · Emmanuel Ngameni[1]

Received: 22 April 2021 / Accepted: 18 July 2021 / Published online: 3 August 2021


## Abstract

A composite material prepared by polymerization of β-cyclodextrin (β-CD) on the surface of natural hydroxyapatite using citric acid as cross linker, was employed as electrode material for the detection of Pb(II). Hydroxyapatite was obtained from bovine bones, following a three-step procedure including pre-calcination, chemical treatment with $(NH_4)_2HPO_4$, and calcination. The structure and morphology of the pristine hydroxyapatite ($NHAP_{P0.5}$) and its functionalized counterpart ($NHAP_{p0.5}$-CA-β-CD) were examined using XRD, FTIR, and SEM. Upon deposition as thin film on a glassy carbon electrode (GCE), the ion exchange ability of $NHAP_{p0.5}$-CA-β-CD was exploited to elaborate a sensitive sensor for the detection of lead. The electroanalytical procedure was based on the chemical accumulation of Pb(II) ions under open-circuit conditions, followed by the detection of the preconcentrated species using differential pulse anodic stripping voltammetry. The reproducibility of the proposed method, based on a series of 8 measurements in a solution containing 2 μM Pb(II) gave a coefficient of variation of 1.27%. Significant parameters that can affect the stripping response of Pb(II) were optimized, leading to a linear calibration curve for lead in the concentration range of $2 \times 10^{-8}$ mol $L^{-1}$ – $20 \times 10^{-8}$ mol $L^{-1}$ ($R^2 = 0.998$). The detection limit (3S/m) and the sensitivity of the proposed sensor were $5.06 \times 10^{-10}$ mol $L^{-1}$ and 100.80 μA.μ$M^{-1}$, respectively. The interfering effect of several ions expected to affect the determination of lead was evaluated, and the proposed sensor was successfully applied in the determination of Pb(II) ions in spring water, well water, river water and tap water samples.

**Keywords** Hydroxyapatite · β-cyclodextrin · Lead · Electroanalysis

Guy B. P. Ngassa and Ignas K. Tonlé contributed equally to this work.

Responsible Editor: Weiming Zhang

✉ Guy B. P. Ngassa
guyngassa@yahoo.fr

✉ Ignas K. Tonlé
ignas.tonle@univ-dschang.or

[1] Laboratory of Analytical Chemistry, Faculty of Science, The University of Yaounde 1, P.O. Box 812, Yaounde, Cameroon

[2] Department of Chemistry, University of Douala, P.O. Box 24157, Douala, Cameroon

[3] Institute of Inorganic Chemistry, Christian-Albrechts-Universität zu Kiel, Max-Eyth-Straβe 2, 24118 Kiel, Germany

[4] Freiburg Materials Research Center (FMF), University of Freiburg, Stefan Meier Strasse 21, 79104 Freiburg, Germany

[5] Chemistry of Materials and Electrochemistry, Faculty of Science, University of Dschang, P.O. Box 67, Dschang, Cameroon

## Introduction

Due to their nonbiodegradability and especially their toxicity, inorganic pollutants such as heavy metals pose a major threat to the environment because of their involvement in many natural and industrial processes (Adebisi et al. 2017). Among heavy metals, lead is particularly toxic, with negative effects on human health. Yet, it is known that the ingestion of lead can induce damages on the nervous system, the main pathologies being severe headaches, encephalopathy, sleepiness, psychosis, memory deterioration, and reduced consciousness (Flora et al. 2012). The safe disposal of lead is always a concern in industrialized countries. The World Health Organization (WHO), the European Union (EU), and the US Environmental Protection Agency (USEPA) set the permissible level of lead in drinking water at 0.01, 0.01 and 0.015 mg $L^{-1}$, respectively (Awual 2019). To quantify and monitor lead ions, the development of analytical devices has attracted

increasing interest in recent decades. For this purpose, a range of different analytical methods have been utilized, such as inductively coupled plasma-mass spectrometry (Longerich et al. 1987), X-ray fluorescence spectrometry (Lau and Ho 1993), and atomic absorption spectrometry (Chen and Teo 2001). These techniques operate quiet well but usually they require expensive equipment, highly trained staff for their implementation, and long time for analyzes. To overcome these limitations, the development of electrochemical techniques based on modified electrodes has been promoted as these techniques can be easily implemented, and are characterized by high selectivity and sensitivity, good repeatability, and cheap instrumentation (Ngassa et al. 2014; Tonle et al. 2015). Moreover, modified electrodes offer the advantage of using several types of electrode materials, depending on their availability and on their specific properties (Fairuz et al. 2016; Musa et al. 2020). This has boosted in the past recent years the development of a wide variety of electrochemical sensors for environmental applications (Shetti et al. 2019; Ilager et al. 2020a; Ilager et al. 2020b; Ilager et al. 2021; Malode et al. 2021). Among the electrode materials used, hydroxyapatite (HAP) with the formula $Ca_{10}(PO_4)_6(OH)_2$ has been shown to be a prominent material. Due to its microcrystalline structure, its acid-base properties, ion-exchange ability, adsorption capacity, and its chemically reactive sites (Chen et al. 2008), HAP is exploited in various fields (Sun et al. 2018; Ajab et al. 2019; El Mhammedi et al. 2009a; Li et al. 2009; Prongmanee et al. 2019). Thus, several studies have reported the use of this material as electrode modifier for the detection of different organic pollutants (El Mhammedi et al. 2007; El Mhammedi et al. 2009a; Li et al. 2009; Yin et al. 2010; Tchoffo et al. 2021). Also, HAP modified electrodes have been applied for the detection of heavy metal ions, including $Pb^{2+}$ (Pan et al. 2009; El Mhammedi et al. 2009b; El Mhammedi et al. 2013), $Cd^{2+}$ (Li et al. 2009; Gao et al. 2016), $Cu^{2+}$, and $Hg^{2+}$ (Sun et al. 2018). HAP can be synthesized via various chemical routes (Sadat-Shojai et al. 2013) such as mechanochemical (Fakharzadeh and Ebrahimi-Kahrizsangi 2017; Youness et al. 2017), precipitation (Horta et al. 2019), hydrothermal (Nouri-Felekori et al. 2019), sol-gel (Turk et al. 2019), and polymer-assisted methods (Sinha et al. 2008; Tseng et al. 2009) that are relatively high in cost (Esmaeilkhanian et al. 2019; Yala et al. 2013). More interesting, HAP can be extracted from several natural sources such as clam shell (Pal et al. 2017), cuttlefish bone (Faksawat et al. 2015; Goto and Sasaki 2016), bovine bones (Hammood et al. 2017; Amna 2018), and corals (Nandi et al. 2015). Several investigations have shown that natural HAP (referred as NHAP hereafter) obtained from these sources is more bioactive and has a more dynamic response to the environment, along with a better metabolic activity compared to the synthetic HAP (Yala et al. 2013; Esmaeilkhanian et al. 2019). NHAP is not only easy to obtain but is also simple to process; in addition it is available in unlimited quantities as bone waste (Yala et al. 2013; Mohd et al. 2019).

HAP has on its surface numerous hydroxyl groups (P-OH and Ca-OH) that can allow their modification by grafting of either organic or inorganic compounds (Saoiabi et al. 2010). Therefore, the modification of HAP surface with various organic substances has been the subject of many studies (Liu et al. 1998; Leprêtre et al. 2009; Othmani et al. 2013; Tang et al. 2013; Yala et al. 2013). These modifications are of great interest as they induce to the material new properties. Among the organic modifiers generally used, natural polymers are increasingly solicited. Nowadays, many reports focus exclusively on β-cyclodextrin (β-CD) which is a natural macrocyclic oligosaccharide composed of seven glucose molecules. It is toroidal in shape, with a hydrophilic outer side which provides water solubility and a hydrophobic inner cavity (Niu et al. 2018; Tcheumi et al. 2019). These interesting characteristics provide the materials functionalized by β-CD a wide field of application, especially in electroanalysis (Alam et al. 2018; Tcheumi et al. 2019; Tchoffo et al. 2021; Yang et al. 2015; Zhu et al. 2016). Thus, Alam et al. (2018) used multiwalled carbon nanotube and β-CD for the electrochemical sensing of acetaminophen. Liu et al. (2017) exploited SH/β-CD functionalized graphene-palladium nanoparticles for the sensitive electrochemical detection of rutin and isoquercitrin. In the recent past years, our research unit is involved in the valorization of β-CD for the protection of environment. In these lines, the exploitation of smectite/β-CD composite material for the detection of paraquat has been achieved (Tcheumi et al. 2019). Also, we have reported the use of a hydroxyapatite/β-CD hybrid material for the electrochemical detection of diquat (Tchoffo et al. 2021). In the framework of that program, the present study describes the electroanalysis and detection of $Pb^{2+}$ ions in aqueous medium. To our knowledge, no study on the use of a composite material based on natural hydroxyapatite and β-CD as electrode modifier for the electrochemical quantification of $Pb^{2+}$ has been reported in the literature. Thus, a simple, sensitive and low cost lead electrochemical sensor was expected by creating a favorable environment on hydroxyapatite surface, for more efficient adsorption of $Pb^{2+}$ ions. This was achieved by immobilizing β-CD molecules bearing complexing functional groups, and citric acid molecules dotted with free carboxylate functions that can uptake $Pb^{2+}$ ions via electrostatic interactions, in addition to the intrinsic cation exchange properties of NHAP.

## Experimental

### Chemicals and reagents

All chemicals and reagents used in both the material synthesis and the electrochemical sections were of analytical grade, and used as received. The 0.01 M stock solution of Pb(II)

(Prolabo) was prepared by dissolving $Pb(NO_3)_2$ in deionized water. $Ru(NH_3)_6Cl_3$ (98%) was purchased from Aldrich. $(NH_4)_2HPO_4$ (Anachemia) was used for the chemical treatment of precursor. β-cyclodextrin (98%, Aldrich), citric acid (99%, Sigma-Aldrich), and $Na_2HPO_4$ (Anachemia) were used for the surface modification of hydroxyapatite. $CH_3COOH$ (99.8%, Scharlau) and $CH_3COONa$ (99%, Synth) were mixed with different ratios for the preparation of the 0.1 M acetate buffer at different pH values. The pH of the accumulation medium was adjusted using dilute solutions of KOH (BDH) or $HNO_3$ (60%, Scharlau). All solutions were prepared with deionized water (18 MΩ. $cm^{-1}$) obtained from a Millipore milli-Q water purification system.

## Preparation and characterization of the β-cyclodextrin/hydroxyapatite composite

### Starting bovine bones material: pre-treatment, calcination and impregnation

The preparation and characterization of β-CD/hydroxyapatite composite material is fully described elsewhere (Tchoffo et al. 2021). Briefly, the starting materials were bovine bones collected at local market. They were carefully cleaned and cut into small pieces of about 2 to 5 cm, then boiled for 30 min in deionized water. The pieces were finally washed several times using water, in order to remove all traces of remaining meat and fat. Upon drying at room temperature for about 30 days, the bone marrow was scraped, and the resulting cleaned bone was pre-calcined in an electric oven with the heating rate set at 12.5 °C.$min^{-1}$; followed by a residence time of 3 h at 450 °C. The bones were cooled slowly to room temperature and the calcined material was then crushed, sieved, and the particles smaller than 50 μm were retained for later use. This pre-calcined material (referred as precursor) was chemically treated as follows: 2 g of precursor were added to 40 mL of a 0.5 M solution of activating agent ($(NH_4)_2HPO_4$) chosen to avoid the destruction of hydroxyapatite structure. The impregnation step was achieved in a glass vial under constant stirring at 150 rpm at (20 ± 2) °C for 48 h. The sample was then washed several times with deionized water, filtered, and then dried in an oven for 24 h at 80 °C. The final material was washed with deionized water until the neutral pH of solution was reached. The fine particles of the impregnated material were then collected. For this purpose, the particles obtained in the previous step were dispersed in 200 mL of deionized water and the suspension was placed in a sedimentation tube, the fraction below 3 μm was separated by sedimentation according to the Stokes law and then recovered by centrifugation. Afterwards, more deionized water was added in the tube and the procedure repeated until a clear liquid was obtained at the top of the tube. The resulting material (hereafter denoted as $NHAP_{P0.5}$) and not impregnated material (hereafter denoted as NHAP) were dried in an oven for 24 h at 80 °C and stored in plastic containers for later use.

### Coupling of β-cyclodextrin to hydroxyapatite

The synthesis of the β-CD natural hydroxyapatite composite was adapted from a published procedure (Leprêtre et al. 2009). An amount of 0.5 g of $NHAP_{P0.5}$ was carefully dispersed in 5 mL deionized water in an ultrasonic bath for 5 min. Afterwards, 0.25 g of β-CD, 0.25 g citric acid (cross linker agent), and 0.083 g of $Na_2HPO_4$ (catalytic agent) were added to this mixture. The mass ratio of β-CD and natural hydroxyapatite was set at 1:2 (w/w). The resulting mixture was sonicated for 5 min and the solution obtained was transferred to an electric oven at 100°C for 120 min. The obtained residue was then placed in an electric oven at 180°C for 45 min, followed by cooling at ambient temperature. The solid residue obtained was carefully crushed, washed with deionized water, and dried in an oven. The final composite material thus synthesized was referred as $NHAP_{P0.5}$-CA-β-CD. All steps involved in the preparation of $NHAP_{P0.5}$-CA-β-CD are given in Scheme 1. For comparison purposes, the same protocol was followed to prepare the β-CD polymer (without hydroxyapatite, denoted CA-β-CD), excepted that natural hydroxyapatite was no longer used.

### Physic-chemical characterization of materials

The structural properties and the morphological structure of the starting hydroxyapatite, the precursor, and the lysine/NHAP materials were determined by Powder X-Ray diffraction (PXRD), Fourier Transformed Infrared (FTIR) spectroscopy and Scanning Electron Microscopy (SEM). The PXRD patterns were recorded at room temperature using powder diffractometer (Stoe Stadi-P) operating with a Cu-Kα radiation (λ = 1.54056 Å). FTIR spectra were registered also at room temperature using KBr pellets, in the spectral range from 4500 to 400 $cm^{-1}$ on an Alpha IR spectrometer from Bruker. SEM images were obtained using an Amray 1610 Turbo instrument.

## Electrochemical experiments

Electrochemical measurements were performed by a computerized Potentiostat instrument (Metrohm μ-Autolab, Netherlands) using the GPES software. All voltammograms were recorded at room temperature with a single compartment three-electrode cell comprising a platinum grid as counter electrode, an Ag/AgCl/KCl (3 M) reference electrode, and a working electrode that was either a bare glassy carbon electrode (GCE), or the GCE modified by a thin film of CA-β-CD, $NHAP_{P0.5}$ or $NHAP_{P0.5}$-CA-β-CD material. The GCE was first polished on billiard cloth covered by alumina paste

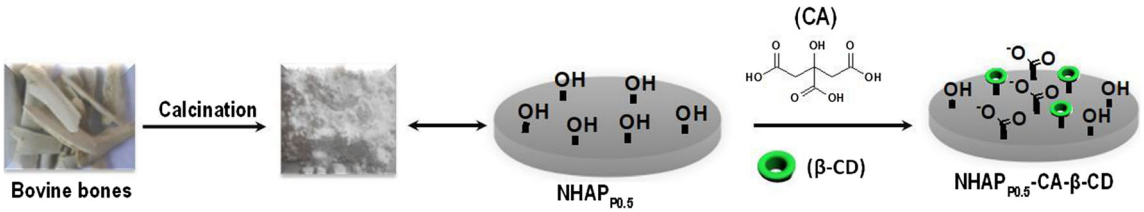


**Scheme 1.** Representation of the successive steps involved in the preparation of β-CD functionalized hydroxyapatite

(0.05 μm particle size), then ultrasonically cleaned for 5 min in deionized water. Dispersions of the materials (NHAP$_{P0.5}$, NHAP$_{P0.5}$-CA-β-CD or CA-β-CD) were prepared by diluting 4 mg of each material in 2 mL of deionized water. Eight microliter of the dispersion was then casted on the active surface (3 mm in diameter) of the GCE. The thin film electrode was dried at room temperature for about 2 h to ensure complete drying, then used without any pre-treatment in the electrochemical cell. These electrodes will be hereafter referred as GCE/NHAP$_{P0.5}$, GCE/CA-β-CD, and GCE/NHAP$_{P0.5}$-CA-β-CD for the GCE modified by NHAP$_{P05}$, CA-β-CD, and NHAP$_{P05}$-CA-β-CD; respectively.

Cyclic voltammetry was used to evaluate the active surface area of the bare GCE and modified electrodes, while the electrochemical analysis of $Pb^{2+}$ ions was carried out using differential pulse anodic stripping voltammetry (DPASV). The procedure was based on two successive steps: (i) the open-circuit accumulation of the analyte was achieved by dipping the working electrode in a beaker kept at constant stirring and containing the $Pb^{2+}$ solution at a given concentration; and (ii) the voltammetric detection of the accumulated analyte between −0.90 and −0.20 V in 0.1 M acetate buffer solution. DPASV measurements were performed by applying the following optimized parameters: 0.00 s equilibration time, 5 mV potential step increments, and 100 mV potential amplitude. After each voltammetric detection and before the next accumulation, the surface of the working electrode was renewed by simply shaking it in the detection medium for approximately 3 min.

## Results and discussion

### Physicochemical characterization of materials

Figure 1A presents the FTIR spectra between 3800 and 380 $cm^{-1}$ of NHAP, NHAP$_{P0.5}$, and NHAP$_{P0.5}$-CA-β-CD materials. On all spectra, fundamental peaks characteristic of hydroxyapatites are observed (Koutsopoulos 2002). The absorption bands which appear around 3450 and 1638 $cm^{-1}$ correspond to the bending vibrations of water molecules adsorbed on the materials (Koutsopoulos 2002; Patel et al. 2015; Kanchana and Sekar 2014). The visible vibration bands of OH groups were identified at 3570 and 630 $cm^{-1}$ (Kanchana and Sekar 2014). The absorption peaks observed at 1458, 1419, and 873 $cm^{-1}$ are attributed to the binding vibrations of carbonate $(CO_3)^{2-}$ in the structure of the material (Koutsopoulos 2002; Kanchana and Sekar 2014). The vibrations bands of phosphate $PO_4^{3-}$ were also detected at 1090, 1039, 961, 601, and 569 $cm^{-1}$, respectively (Yala et al. 2013; Koutsopoulos 2002). On the basis of these results, it can be deduced that all the collagens and other organic compounds present in the raw bones have been eliminated during calcination. After treatment with dibasic ammonium phosphate, the spectrum of the resulting material (NHAP$_{P0.5}$) displays bands similar to those of NHAP. This confirms that this treatment had not affected the structure of the material. Furthermorer, comparing the spectra of pristine HAP and NHAP$_{P0.5}$-CA-β-CD samples clearly showed additional peaks at 2933 and 1729 $cm^{-1}$ that are respectively attributed to the vibrations bands of C-H groups of β-CD and C=O bands of ester bonds formed during the polymerization (Leprêtre et al. 2009; Tang et al. 2013; Tcheumi et al. 2019; Heydari and Sheibani 2015). The observed absorption bands of ester groups indicated that hydroxyl groups of β-CD have reacted with the carboxyl groups of citric acid, leading to the formation of a three-dimensional polymer network (Tcheumi et al. 2019).

The crystalline phase analyzes of obtained materials were carried out by XRD as shown in Fig. 1B. The pattern of NHAP starting material (Fig. 1B(a)) presents well-defined and thin diffraction peaks, proving that the material has a good crystallinity. Some typical and specific crystallographic plane (002), (102), (112), (211), (300), (130), (202), and (310) appearing at 25.80°, 28.92°, 31.71°, 32.21°, 32.90°, 34.13°, 40°, 46.70°, and 49.44° 2θ angles were matched with standard ICDD Diffraction File No. 00-009-0432 of hydroxyapatite (Kanchana and Sekar 2014). This confirms the results obtained in FTIR, from which it appeared that the material obtained from bovine bones after calcination was pure hydroxyapatite.

Upon the impregnation of NHAP with ammonium phosphate dibasic, the material becomes somewhat amorphous (Fig. 1B(b)) although the main diffraction peaks remain visible. By comparing the XRD pattern of the hybrid material (NHAP$_{P0.5}$-CA-β-CD) with that of unmodified hydroxyapatite (NHAP$_{P0.5}$), it can be seen that the characteristic diffractions of two materials are almost the same, which shows that the grafting of β-CD had not affected the crystalline phases of the hydroxyapatite particles as previously observed by Leprêtre et al. (2009) in similar materials. By exploiting the Scherrer's equation (Elkabouss et al. 2004) expressed by $D = K.\lambda.(\beta.\cos\theta)^{-1}$ where K is the shape factor

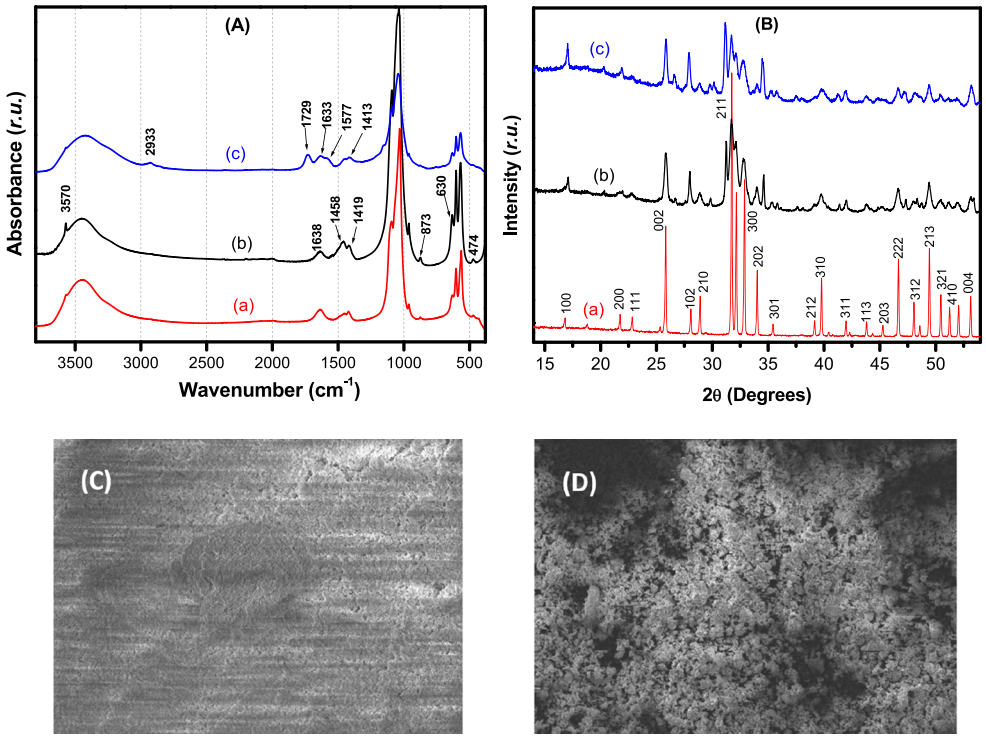


**Fig. 1** **A** FTIR spectra, **B** PXRD patterns of (a): NHAP, (b): NHAPP0.5 and (c): NHAPP0.5-CA-ß-CD materials; SEM pictures of **C** $NHAP_{P0.5}$ and **D** $NHAP_{P0.5}$-CA-β-CD materials

(0.9), β the full width at half-maximum of diffraction peaks measured in radians, λ the wavelength of the used anticathode ($\lambda_{Cu}$ = 1.54056Å), and θ is Bragg's diffraction angle, the average crystallite size of NHAP, $NHAP_{P0.5}$, and $NHAP_{P0.5}$-CA-β-CD were estimated as 279.65, 36.61, and 99.22 nm, respectively. The treatment of NHAP with dibasic ammonium phosphate induces a significant reduction of the crystal size. Yet, this treatment caused a structural reorganization of the material making it better dispersed. When the treated material was functionalized with β-CD, particle size increased, probably due to the grafting of β-CD on the surface of the material.

SEM was used to examine the morphological structure of the pristine hydroxyapatite ($NHAP_{P0.5}$) and its functionalized counterpart ($NHAP_{p0.5}$-CA-β-CD). Figures 1C and 1D present the obtained images. It was noticed that the natural hydroxyapatite particles, after chemical impregnation are characterized by an irregular shape (Fig. 1C). The morphology exhibited a porous network remaining after the removal of organic materials from the bones. The functionalization of the natural hydroxyapatite with β-CD (Fig. 1D) led to better dispersed particles of the obtained material. Many micropores also appeared on this material, probably making available the free acid groups of citric acid not involved in the grafting process.

## Preliminary electrochemical investigations

A preliminary investigation was performed in view of selecting the most sensitive material to be used as GCE modifier for the electrochemical sensing of $Pb^{2+}$ ions, the ability of the prepared materials was investigated. Thus, GCE/$NHAP_{P0.5}$, GCE/CA-β-CD, and GCE/$NHAP_{P0.5}$-CA-β-CD devices were used in turn to analyze a $2 \times 10^{-6}$ M $Pb^{2+}$ solution, and the DPASV curves obtained are shown in Fig. 2. As one can observe, a peak current of about 14.04 μA in intensity was generated at the GCE electrode modified by raw hydroxyapatite ($NHAP_{P0.5}$). This signal is due to the ability of hydroxyapatite to easily adsorb positive ions by a cation exchange mechanism (El Mhammedi et al. 2009b; Mobasherpour et al. 2011).

When the bare GCE was modified by β-cyclodextrin polymer, the anodic peak current obtained was enhanced (23.98 μA), giving rise to intensity more than 1.7-fold larger than that obtained in the same conditions on GCE/$NHAP_{P0.5}$. This result is due in one hand to the capacity of β-CD to form reversible inclusion complexes with $Pb^{2+}$metal ions (Zhao et al. 2019), and in the other hand to the ability of the free carboxylate functions of citric acid to trap $Pb^{2+}$ ions (He et al. 2017; Celebioglu et al. 2019). Finally, when the film on the GCE was formed by the composite material ($NHAP_{P0.5}$-CA-β-CD), the anodic peak current obtained was substantially improved. The peak current obtained (38.60 μA) was 1.61-fold and 2.75-fold more intense than the signals recorded on GCE/CA-β-CD and GCE/$NHAP_{p0.5}$, respectively. This observation can be reasonably attributed to three major factors: (i) the complexation of $Pb^{2+}$ ions by β-CD; (ii) the ability of free carboxylate functions of citric acid that can also contribute by electrostatic attraction to accumulate $Pb^{2+}$ ions; and (iii) the

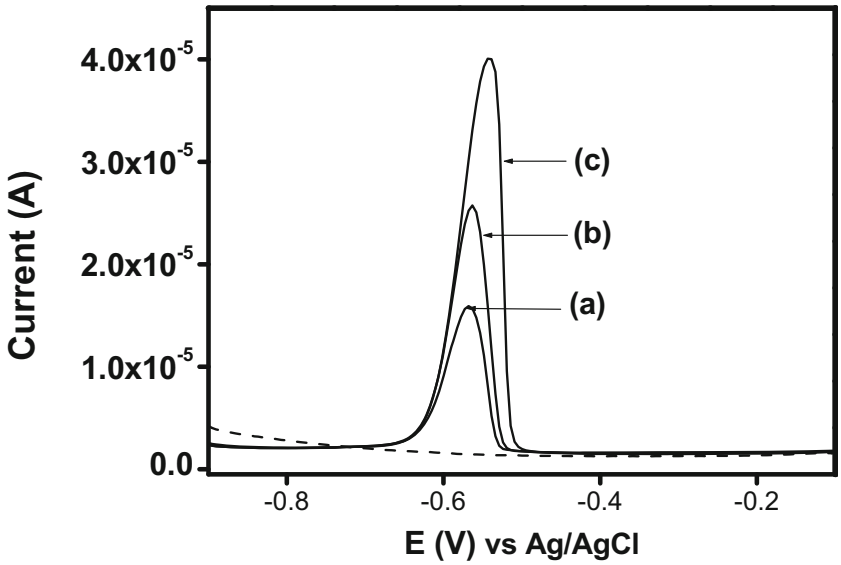


**Fig. 2** DPASV recorded after 3 min accumulation from an aqueous $2 \times 10^{-6}$ M $Pb^{2+}$ solution at pH 6 using, **a** GCE/$NHAP_{P05}$, **b** GCE/CA-β-CD, and **c** GCE/$NHAP_{P05}$-CA-β-CD. Detection in 0.1 M acetate buffer (pH 5) after 15 s electrolysis at −0.8 V. Other experimental conditions: 0 s equilibration time, 5 mV potential step and 100 mV amplitude

adsorption of $Pb^{2+}$ ions by natural hydroxyapatite present in the film, following an ion exchange process. From these investigations, the composite material was thus chosen for further experiments as it led to the most sensitive detection of $Pb^{2+}$ ions.

Furthermore, it was useful to determine the exposed surface area of the GCE before and after its modification by the thin film of $NHAP_{P0.5}$-CA-β-CD material. Thus, the effective surface area of GCE and GCE/$NHAP_{P0.5}$-CA-β-CD was measured using the following Randles-Sevcik equation (Bukkitgar and Shetti 2017; Shetti et al. 2015).

$$\mathrm{Ipa} = \left(2.69 \times 10^{5}\right) n^{3/2} A_0 D_0{}^{1/2} \upsilon^{1/2} C_0 \quad (1)$$

where Ipa refers to the anodic peak current (A), n is the number of electrons transferred during the electrode reaction, $A_0$ represents the working surface area of the electrode ($cm^2$), $D_0$ is the diffusion coefficient ($8.43 \times 10^{-6}$ $cm^2$ $s^{-1}$ for $[Ru(NH_3)_6]^{3+}$ ion), υ is the scan rate (V $s^{-1}$), and $C_0$ is the concentration of $[Ru(NH_3)_6]^{3+}$ (mol $cm^{-3}$). Experiments were performed by cyclic voltammetry in a 0.1 M KCl supporting solution containing $1 \times 10^{-3}$ M $[Ru(NH_3)_6]^{3+}$ as redox probe, at different scan rates. From the plot of Ipa *vs* υ, the active surface area of the bare GCE was calculated to be 0.061 $cm^2$ whereas the area of $NHAP_{P0.5}$-CA-β-CD modified GCE was found to be 0.181 $cm^2$.

The reproducibility and stability of the composite material coated on the GCE were then evaluated. For this purpose, a series of 8 repetitive measurements were performed by using the same GCE/$NHAP_{P0.5}$-CA-β-CD sensor for the detection of 2 μM $Pb^{2+}$ ions. As shown on Fig. SI(1) (Electronic Supporting Material), highly reproducible stripping currents were obtained with a relative standard deviation of 1.27%. Moreover, a series of measurements on five electrodes prepared with an identical procedure gave a relative standard deviation of 3.75%. This indicates a good reproducibility of the proposed sensor for the detection of $Pb^{2+}$ ions. The long-term stability of the proposed sensor was also evaluated by recording daily the signal of a 2 μM $Pb^{2+}$ solution, the electrode being kept in 0.1 M acetate buffer (pH 5) in a fridge. It was found that GCE/$NHAP_{P0.5}$-CA-β-CD can retain more than 96% of its original response, without regenerating or reactivating the surface during the process of successive determinations. In order to obtain the highest sensitivity of the modified electrode for the electrochemical determination of $Pb^{2+}$, the operating parameters of the accumulation and detection steps have been optimized in the coming sections.

## Optimization of key parameters involved in the accumulation step

The pH of the accumulating medium is an important parameter, expected to affect the electrode signal. It was investigated on GCE/$NHAP_{P0.5}$-CA-β-CD in the range between 4.0 and 6.5 by DPASV in aqueous solution containing 2μM of $Pb^{2+}$. It is important to mention that in highly acidic media (pH < 3), no real signal was obtained, probably due to the mineralization of the hydroxyapatite backbone. Basic media were not studied as they may induce the precipitation of $Pb^{2+}$. The obtained results are given in Fig. 3A: in moderate acidic media, the stripping peak current of $Pb^{2+}$ increased as the pH was changed from 4.0 to 5.0, then it decreased to 6.5. The poor sensor signal obtained for pH values less than 4 was attributed to a competition between $H^+$ and the $Pb^{2+}$ ions, and to the protonation of the free carboxylic acid functions available on the surface of the composite material. As noticed, the optimal pH for the detection of $Pb^{2+}$ ions is 5, that was chosen for further investigations.

The duration of the accumulation step is the second factor that can influence the sensor response. It was thus necessary to study its effect on the peak current of $Pb^{2+}$. The DPASV curves recorded at GCE/$NHAP_{P0.5}$-CA-β-CD dipped in an aqueous solution (pH 5) containing 2 μM $Pb^{2+}$ for accumulation time varied between 1 and 30 min are shown in Fig. 3B. It can be noted the peak current increased linearly with increasing accumulation time up to 8 min, showing a rapid and progressive occupation of the binding sites on the working electrode. Afterwards, the peak current leveled as these sites are almost all occupied. For further measurements, an accumulation time of 600 s was employed.

## Optimization of the detection parameters

### pH of the detection solution

Since the deposition of $Pb^{2+}$ ions on GCE/$NHAP_{P0.5}$-CA-β-CD strongly depends on the pH, the effect of the acidity of the detection solution on the stripping peak current was studied in 0.1 mol $L^{-1}$ acetate buffer with pH ranging from 3.5 to 6.5. The results given in Fig. 4A show that the pH of the detection medium greatly affects the peak current of $Pb^{2+}$ as reported by some previous studies (Lv et al. 2013; Mohammadi et al. 2020). From Fig. 4B, the electrode response increased from pH 3.5 to reach a maximum at pH 5, then decreased for pH value between 5 and 6.5. Thus, pH 5 was selected as optimum value and used in coming sections.

### Deposition potential and electrolysis time

In electroanalysis technique based on adsorptive stripping voltammetry, the deposition potential and it duration are determining factors to achieve high sensitivity. The effect of both parameters was studied and the data obtained are shown on Fig. 5. Varying the deposition potential in the range from −0.1 to −1.0 V revealed that the peak currents increased slightly when the deposition potential was decreased from 0 to −0.5 V, then increased significantly for potential values between −0.6 V and −0.8 V, to stabilize beyond (Fig. 5A). Thus, for a quantitative reduction of $Pb^{2+}$ ions, the deposition should be operated at a potential lying between −0.8 V and −1.0 V.

Futhermore, the effect deposition duration on the electrode signal of 2 μM $Pb^{2+}$ was investigated in the range from 0 to 30 s (after 3 min of preconcentration). The results on Fig. 5B indicated that the electrode signal increased rapidly with the electrolysis time to reach a maximum from 20 s. This phenomenon is ascribed to the progressive and rapid occupation of the analyte on the accumulation sites at the working electrode. Upon saturation of these sites, the peak current became constant. Therefore, for subsequent experiments, the deposition of $Pb^{2+}$ ions was achieved at −0.8 V for 30 s.

## Influence of lead concentration and calibration curve

By using the optimized parameters selected in previous sections on the optimization of accumulation and detection steps, DPASV experiment were conducted for $Pb^{2+}$ concentration varied between $2.00 \times 10^{-8}$ mol $L^{-1}$ and $20.00 \times 10^{-8}$ mol $L^{-1}$. As shown in Fig. 6, the stripping peak current increased with increasing $Pb^{2+}$ concentration. As shown by the inset in Fig. 6, a linear relationship was obtained for the peak current (Ip) and concentration of $Pb^{2+}$, which obeyed to the following equation:

$$\mathrm{Ip}(\mu\mathrm{A}) = 100.80\left[\mathrm{Pb}^{2+}\right](\mu\mathrm{M}) + 0.15 \times 10^{-6} \quad \left(R^2 = 0.998\right) \tag{2}$$

The sensitivity of the electrode was 100.80 μA.$\mu M^{-1}$, while a limit of detection of $5.06 \times 10^{-10}$ mol $L^{-1}$ was calculated for a signal-to-noise ratio equal to 3.

Such analytical performances of GCE/$NHAP_{P0.5}$-CA-β-CD sensor for $Pb^{2+}$ detection were confronted with some other electrochemical sensors, and the data were summarized in Table 1.

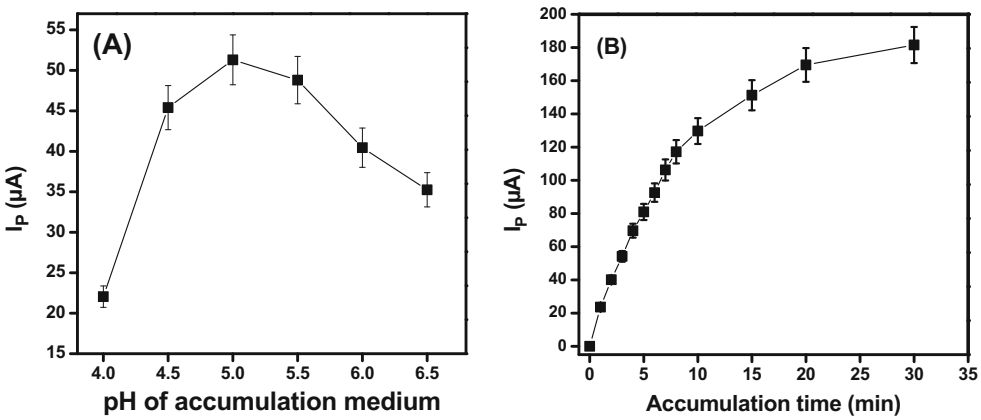


**Fig. 3** **A**: Evolution of peak current at GCE/$NHAP_{P0.5}$-CA-β-CD as a function of the pH of accumulating medium, after 3 min accumulation from a 2 μM $Pb^{2+}$ aqueous solution. **B** Effect of accumulation time on the current recorded at GCE/$NHAP_{P0.5}$-CA-β-CD in aqueous solution (pH 5) containing 2 μM $Pb2^{+}$. Detection in 0.1 M acetate buffer (pH 5) after 30 s electrolysis at −0.8 V

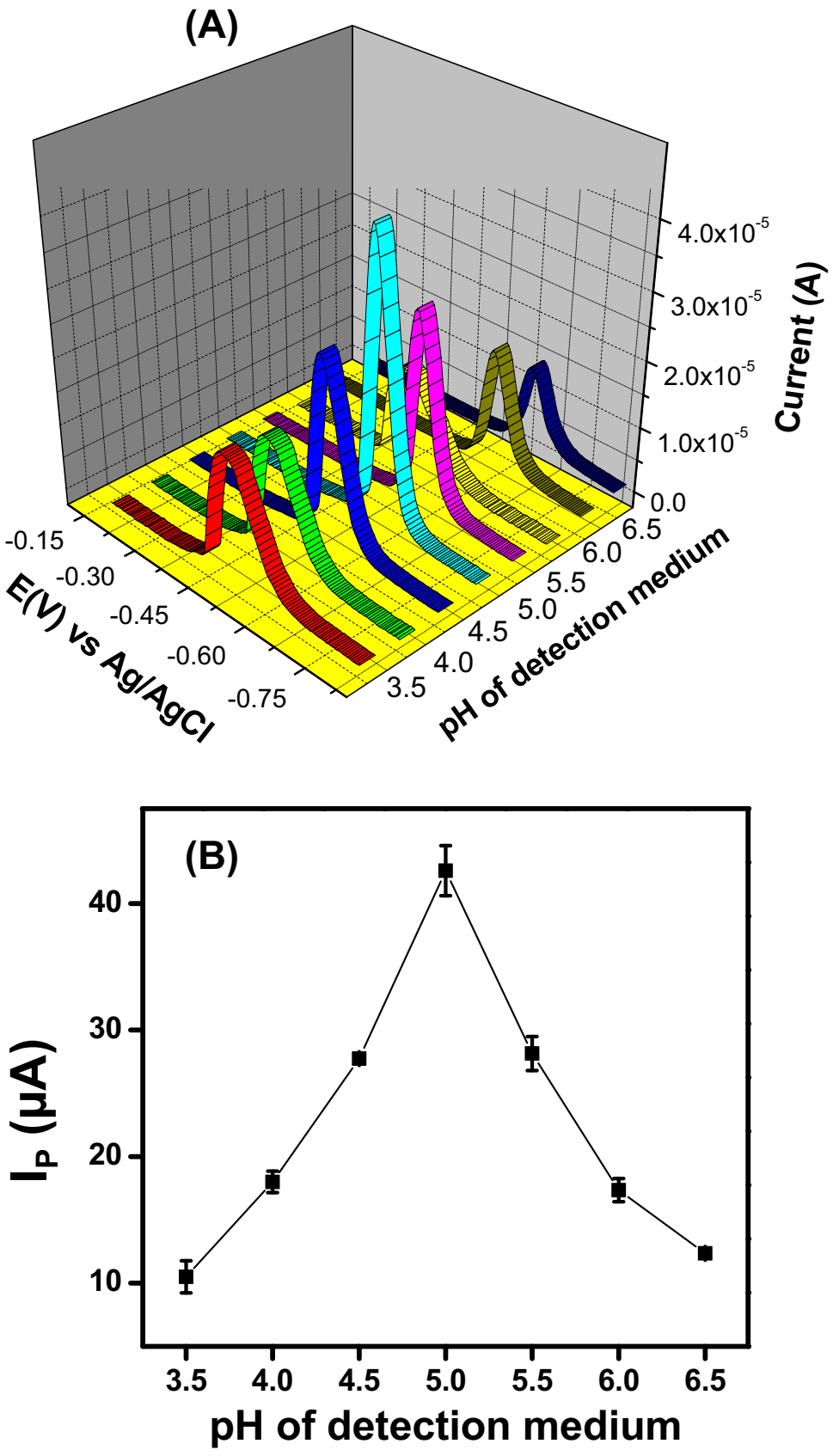


**Fig. 4** **A**: DPASV recorded at GCE/$NHAP_{P0.5}$-CA-β-CD for different pH of detection medium after 3 min accumulation from an aqueous $2 \times 10^{-6}$ M $Pb^{2+}$ solution (pH 6). Detection after 15 s electrolysis at −0.8 V. (**B**): the corresponding peak current variation

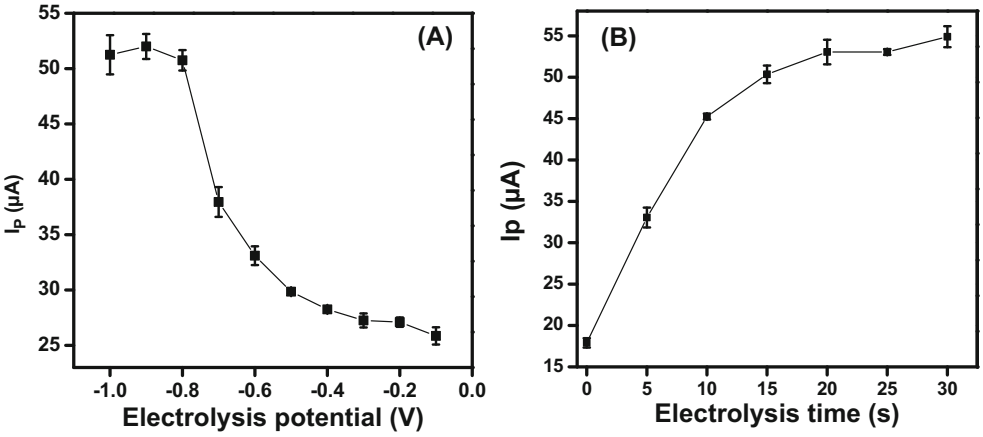


**Fig. 5.** **A**: Dependence of Pb(II) peak current on electrolysis potential, after 3 min preconcentration in 2 µM $Pb^{2+}$ (pH 5), on GCE/$NHAP_{P0.5}$-CA-β-CD. Detection in 0.1 M acetate buffer (pH 5) after 15 s electrolysis. **B**: Variation of Pb(II) peak intensities at GCE/$NHAP_{P0.5}$-CA-β-CD with electrolysis duration. Other conditions as in (A)

By analyzing these data, it appears that the analytical performance of GCE/$NHAP_{P0.5}$-CA-β-CD is better in comparison with some previously reported sensors (El Mhammedi et al. 2009b; Pan et al. 2009; Li et al. 2016; Mohammadi et al. 2020; Oliveira et al. 2020; Xu et al. 2020), or relatively low (Lv et al. 2013; Zhan et al. 2016). However, considering the low cost of the electrode material and the simplicity of preparation of the working electrode, the electrochemical analysis method developed in this work is an efficient and cost-effective for the detection of lead. In addition, the detection limit achieved herein is much lower than $4.83 \times 10^{-8}$ mol $L^{-1}$, the value recommended by the World Health Organization (Awual 2019). This suggested that the method developed in this work could be applied to the monitoring and quantification of $Pb^{2+}$ in food and in aqueous environment.

## Interference study and real sample determination

The selectivity of the sensor was tested under optimal conditions, by analyzing the effect of potential interfering cations and anions on the detection of $Pb^{2+}$ ions. Thus, each of the selected ions was intentionally introduced at known concentrations into the accumulation solution containing 2 µM $Pb^{2+}$. After 3 min preconcentration at open-circuit, the electrode response was recorded and compared to that of $Pb^{2+}$ previously registered alone in the same conditions. The results obtained are summarized in Table 2. As observed, the studied chemical species did not interfere when their concentration was less than $Pb^{2+}$ concentration.

However, for much higher concentrations (about 10-fold), a decrease in the expected current was noticed for some ions. Indeed, there was a current drop, for about 3.47% for $Cd^{2+}$, 2.70% for $Ni^{2+}$, and 50.76% for $Cu^{2+}$. This observation can be explained by the relative good affinity displayed by these ions toward the carboxylate groups of free carboxylic acid present on the composite material (He et al. 2017; Celebioglu et al. 2019). It also appeared that for $K^+$, $Mg^{2+}$, $SO_4^{2-}$, and $Cl^-$ the electrochemical response of $Pb^{2+}$ was slightly disturbed, even for concentrations 100-fold greater.

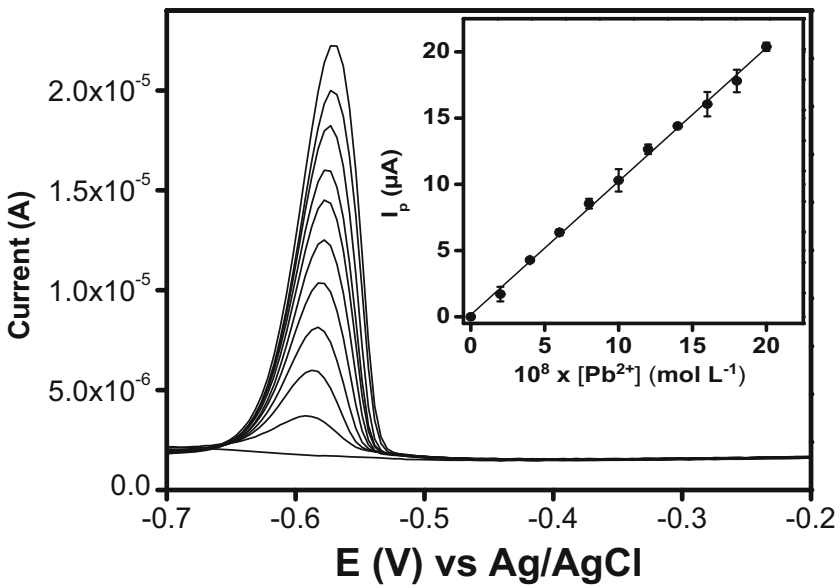


**Fig. 6.** DPASV signal recorded at GCE/$NHAP_{P0.5}$-CA-β-CD under optimized conditions, after 10 min accumulation in an aqueous medium containing $Pb^{2+}$ in the range from $2 \times 10^{-8}$ to $2 \times 10^{-7}$ M. Other experimental conditions are as follows: 0 s equilibration time, 5 mV potential step and 100 mV amplitude. The inset shows the corresponding calibration curve

**Table 1** Comparison of the performance of some recent modified electrodes, towards the voltammetric detection of lead (II)

| Electrode configuration | [a]LOD ($mol.L^{-1}$) | Linear range ($mol.L^{-1}$) | Reference |
|---|---|---|---|
| $Ca_{10}(PO_4)_6(OH)_2$ modified [b]CPE | $7.68 \times 10^{-8}$ | $2.0 \times 10^{-9} - 2.4 \times 10^{-7}$ | El Mhammedi et al. 2009b |
| Nanosized HA nafion modified [c]GCE | $1.00 \times 10^{-9}$ | $5.0 \times 10^{-9} - 8.0 \times 10^{-7}$ | Pan et al. 2009 |
| β-CD[d] reduced GO[e] hybrid nanosheets | $9.42 \times 10^{-11}$ | $1.0 \times 10^{-10} - 9.0 \times 10^{-9}$ | Lv et al. 2013 |
| CPE modified with magnetic eggshell nanocomposite and [f]MWCNTs | $4.52 \times 10^{-7}$ | $1.5 \times 10^{-6} - 6.0 \times 10^{-4}$ | Mohammadi et al. 2020 |
| GCE modified with β-CD and chemically reduced GO | $5.00 \times 10^{-10}$ | $1.0 \times 10^{-9} - 1.0 \times 10^{-7}$ | Zhan et al. 2016 |
| GCE modified with conductive polypyrrole nanoparticles | $55.00 \times 10^{-9}$ | $1.0 \times 10^{-7} - 50.0 \times 10^{-6}$ | Xu et al. 2020 |
| **GCE covered by Zinc oxide nanofibers functionalized by L-cysteine** | $1.20 \times 10^{-9}$ | $3.0 \times 10^{-8} - 4.2 \times 10^{-7}$ | Oliveira et al. 2020 |
| GCE covered by engineered MWCNTs | $1.88 \times 10^{-8}$ | $0.4 \times 10^{-6} - 80.0 \times 10^{-6}$ | Li et al. 2016 |
| GCE modified with β-CD hydroxyapatite composite | $5.06 \times 10^{-10}$ | $2.0 \times 10^{-8} - 2.0 \times 10^{-7}$ | This work |

[a] LOD: Limit of detection
[b] CPE: Carbon paste electrode
[c] GCE: Glassy carbon electrode
[d] β-CD: β-cyclodextrin
[e] GO: Graphene oxide
[f] MWCNT: Multi-walled carbon nanotubes

**Table 2** Variation in the peak current of 2 μM $Pb^{2+}$, recorded in the absence (100%) and in the presence of others ionic species introduced in relation to $Pb^{2+}$ ions concentration

| Interference ions | Added amount over $Pb^{2+}$ concentration | Variation (%) in the peak current of $Pb^{2+}$ ions |
|---|---|---|
| $Cd^{2+}$ | 0.1 | 101.3 |
| | 1 | 98.60 |
| | 10 | 96.53 |
| $Ni^{2+}$ | 0.1 | 102.65 |
| | 1 | 96.96 |
| | 10 | 97.30 |
| $Cu^{2+}$ | 0.1 | 99.14 |
| | 1 | 101.11 |
| | 10 | 49.24 |
| $K^{+}$ | 1 | 100.24 |
| | 10 | 101.30 |
| | 100 | 96.70 |
| $Mg^{2+}$ | 1 | 103.60 |
| | 10 | 99.24 |
| | 100 | 98.10 |
| $SO_4^{2-}$ | 1 | 103.60 |
| | 10 | 99.24 |
| | 100 | 98.10 |
| $Cl^{-}$ | 1 | 100.24 |
| | 10 | 101.30 |
| | 100 | 96.70 |

**Table 3** Recoveries of $Pb^{2+}$ in spring water, well water, river water and tap water samples at GCE/$NHAP_{P0.5}$-CA-β-CD

| | Added ($10^{-7}$ mol $L^{-1}$) | Found[a] ($10^{-7}$ mol $L^{-1}$) | Recovery (%) |
|---|---|---|---|
| Spring water | 1.5 | (1.45 ± 0.04) | 96.67 |
| Well water | 1.5 | (1.47 ± 0.04) | 98.00 |
| River water | 1.5 | (1.43 ± 0.06) | 95.33 |
| Tap water | 1.5 | (1.46 ± 0.03) | 97.33 |

[a] Number of samples assayed = 3

In order to evaluate the potential application of GCE/$NHAP_{P0.5}$-CA-β-CD sensor, the detection of $Pb^{2+}$ ions in spring water, well water, river water and tap water samples (all collected in downtown Yaounde, Cameroon) was conducted. A volume of 50 mL of each sample was taken and used without further treatment as the accumulation medium. It should be noted that for both real samples, no $Pb^{2+}$ signal was found in operational conditions, indicating the absence of any trace of $Pb^{2+}$ ion above the detection limit previously obtained. The determination by DPASV of $Pb^{2+}$ was thus performed using the optimized parameters, by the standard addition method. Each sample was spiked with $1.5 \times 10^{-7}$ mol $L^{-1}$ $Pb^{2+}$ and analyzed in triplicate, and the results achieved are listed in Table 3. The obtained values are in good agreement with the spiked ones, indicating that the proposed method could serve for the determination of lead (II) in real samples.

## Conclusion

A novel and sensitive sensor for $Pb^{2+}$ detection, based on a glassy carbon electrode modified by a thin of hydroxyapatite/β-cyclodextrin composite material was proposed. The organohydroxyapatite exploited as electrode modifier was synthesized by grafting β-cyclodextrin on the surface of natural hydroxyapatite, using citric acid as a cross-linked. Upon, physic-chemical characterization by several techniques, the hydroxyapatite-based composite was used to build a highly sensitive, selective, and reliable sensor that was successfully applied for the electrochemical determination of $Pb^{2+}$ ions in spring water, well water, river water, and tap water samples. Considering the results obtained, this study demonstrated the resort to hydroxyapatite as low-cost for the preparation of analytical devices that may find application in pollution control and environment protection.

**Supplementary Information** The online version contains supplementary material available at https://doi.org/10.1007/s11356-021-15578-8.

**Acknowledgements** IKT acknowledges the support of the Alexander von Humboldt foundation (Germany).

**Availability of data and materials** Not applicable.

**Authors contributions** Rodrigue Tchoffo: data collection and formal analysis. Guy BP Ngassa: conceptualization and original draft writing. Giscard Doungmo: lab investigation. Arnaud T. Kamdem: data collection and analysis. Ignas K. Tonle: writing and editing, funding acquisition. Emmanuel Ngameni: project administration, supervision.

**Funding** This work was funded by the International Science Program (ISP, Sweden), via the support of the African Network of Electroanalytical Chemists (ANEC).

## Declarations

**Ethics approval and consent to participate** Not applicable.

**Competing interests** The authors declare no competing interests.

## References

Adebisi GA, Chowdhury ZZ, Alaba PA (2017) Equilibrium, kinetic, and thermodynamic studies of lead ion and zinc ion adsorption from aqueous solution onto activated carbon prepared from palm oil mill effluent. J Clean Prod 148:958–968. https://doi.org/10.1016/j.jclepro.2017.02.047

Ajab H, Khan AAA, Nazir MS (2019) Cellulose-hydroxyapatite carbon electrode composite for trace plumbum ions detection in aqueous and palm oil mill effluent: interference, optimization and validation studies. Environ Res 176:108563–108569. https://doi.org/10.1016/j.envres.2019.108563

Alam AU, Qin Y, Howlader MMR, Hu NX, Deen MJ (2018) Electrochemical sensing of acetaminophen using multi-walled carbon nanotube and β-cyclodextrin. Sensors Actuators B Chem 254:896–909. https://doi.org/10.1016/j.snb.2017.07.127

Amna T (2018) Valorization of bone waste of Saudi Arabia by synthesizing hydroxyapatite. Appl Biochem Biotechnol 186:779–788. https://doi.org/10.1007/s12010-018-2768-5

Awual MR (2019) An efficient composite material for selective lead (II) monitoring and removal from wastewater. J Environ Chem Eng 7(3):103087. https://doi.org/10.1016/j.jece.2019.103087

Bukkitgar SD, Shetti NP (2017) Fabrication of a TiO 2 and clay nanoparticle composite electrode as a sensor. Anal Methods 9(30):4387–4393. https://doi.org/10.1039/C7AY01068K

Celebioglu A, Toput F, Yildiz ZI, Uyar T (2019) Efficient removal of polycyclic aromatic hydrocarbons and heavy metals from water by electrospun nanofibrous polycyclodextrin membranes. ACS Omega 4:7850–7860. https://doi.org/10.1021/acsomega.9b00279

Chen J, Teo KC (2001) Determination of cadmium, copper, lead and zinc in water samples by flame atomic absorption spectrometry after

cloud point extraction. Anal Chim Acta 540:215–222. https://doi.org/10.1016/S0003-2670(01)01367-8

Chen W, Huang Z, Liu Y, He Q (2008) Preparation and characterization of a novel solid base catalyst hydroxyapatite loaded with strontium. Catal Commun 9:516–521. https://doi.org/10.1016/j.catcom.2007.02.011

El Mhammedi MA, Bakasse M, Chtaini A (2007) Square-Wave Voltammetric Determination of Paraquat at Carbon Paste Electrode Modified with Hydroxyapatite. Electroanalysis 19:1727–1733. https://doi.org/10.1002/elan.200703927

El Mhammedi MA, Achak M, Bakasse M, Chtani A (2009a) Electrochemical determination of para-nitrophenol at apatite-modified carbon paste electrode: application in river water samples. J Hazard Mater 163:323–328. https://doi.org/10.1016/j.jhazmat.2008.06.126

El Mhammedi MA, Achak M, Chtaini A (2009b) $Ca_{10}(PO_4)_6(OH)_2$ modified carbon-paste electrode for the determination of trace lead (II) by square-wave voltammetry. J Hazard Mater 160:55–61. https://doi.org/10.1016/j.jhazmat.2008.03.057

El Mhammedi MA, Achak M, Bakasse M (2013) Evaluation of a platinum electrode modified with hydroxyapatite in the lead(II) determination in a square wave voltammetric procedure. Arab J Chem 6:299–305. https://doi.org/10.1016/j.arabjc.2010.10.010

Elkabouss K, Kacimi M, Ziyad M, Ammar S, Verduraz FB (2004) Cobalt-exchanged hydroxyapatite catalysts: magnetic studies, spectroscopic investigations, performance in 2-butanol and ethane oxidative dehydrogenations. J Catal 226:16–24. https://doi.org/10.1016/j.jcat.2004.05.007

Esmaeilkhanian A, Sharifianjazi F, Abouchenari A, Rouhani A, Parvin N, Irani M (2019) Synthesis and Characterization of Natural Nano-hydroxyapatite Derived from Turkey Femur-Bone Waste. Appl Biochem Biotechnol 189:919–932. https://doi.org/10.1007/s12010-019-03046-6

Fairuz L, Mohd RS, Mohamad NS, Abdul MHR, Nodeh (2016) Electrochemical determination of 24-dichlorophenol at β-cyclodextrin functionalized ionic liquid modified chemical sensor: voltammetric and amperometric studies. RSC Advances 6(102):100186–100194. https://doi.org/10.1039/C6RA19816C

Fakharzadeh A, Ebrahimi-Kahrizsangi R (2017) Effect of dopant loading on the structural features of silver-doped hydroxyapatite obtained by mechanochemical method. Ceram Int 43:12588–12598. https://doi.org/10.1016/j.ceramint.2017.06.136

Faksawat K, Sujinnapram S, Limsuwan P, Hoonnivathana E, Naemchanthara K (2015) Preparation and characteristic of hydroxyapatite synthesized from cuttlefish bone by precipitation. Method Adv Mat Res 1125:421–425. https://doi.org/10.4028/www.scientific.net/AMR.1125.421

Flora G, Gupta D, Tiwari A (2012) Toxicity of lead: a review with recent updates. Interdiscip Toxicol 5:47–58. https://doi.org/10.2478/v10102-012-0009-2

Gao F, Gao N, Nishitani A, Tanaka H (2016) Rod-like hydroxyapatite and Nafion nanocomposite as an electrochemical matrix for simultaneous and sensitive detection of $Hg^{2+}$, $Cu^{2+}$, $Pb^{2+}$ and $Cd^{2+}$. J Electroanal Chem 775:212–218. https://doi.org/10.1016/j.jelechem.2016.05.032

Goto T, Sasaki K (2016) Synthesis of morphologically controlled hydroxyapatite from fish bone by urea-assisted hydrothermal treatment and its $Sr^{2+}$ sorption capacity. Powder Technol 292:314–322. https://doi.org/10.1016/j.powtec.2016.01.041

Hammood AS, Hassan SS, Alkhafagy MT (2017) Access to Optimal Calcination Temperature for Nanoparticles Synthesis from Hydroxyapatite Bovine Femur Bone Waste. Nano Biomed Eng 3:228–235. https://doi.org/10.5101/nbe.v9i3

He J, Li Y, Wang C, Zhang K, Lin D, Kong L, Liu J (2017) Rapid adsorption of Pb, Cu and Cd from aqueous solutions by β-cyclodextrin polymers. Appl Surf Sci 426:29–39. https://doi.org/10.1016/j.apsusc.2017.07.103

Heydari A, Sheibani H (2015) Fabrication of poly (β-cyclodextrin-co-citric acid)/bentonite clay nanocomposite hydrogel: thermal and absorption properties. RSC Adv 5:82438–82449. https://doi.org/10.1039/C5RA12423A

Horta M, Aguilar M, Moura F, Campos J, Ramos V, Quizunda A (2019) Synthesis and characterization of green nanohydroxyapatite from hen eggshell by precipitation method. Mater Today Proceed 14:716–721. https://doi.org/10.1016/j.matpr.2019.02.011

Ilager D, Seo H, Shetti NP, Kalanur SS, Aminabhavi TM (2020a) Electrocatalytic detection of herbicide, amitrole at $WO_3{\cdot}0.33H_2O$ modified carbon paste electrode for environmental applications. Sci Total Environ 743:140691. https://doi.org/10.1016/j.scitotenv.2020.140691

Ilager D, Seo H, Shetti NP, Kalanur SS (2020b) CTAB modified Fe-$WO_3$ as an electrochemical detector of amitrole by catalytic oxidation. J Environ Chem Eng *8*(6):104580. https://doi.org/10.1016/j.jece.2020.104580

Ilager D, Seo H, Kalanur SS, Shetti NP, Aminabhavi TM (2021) A novel sensor based on $WO_3{\cdot}0.33H_2O$ nanorods modified electrode for the detection and degradation of herbicide, carbendazim. J Environ Manag 279:111611. https://doi.org/10.1016/j.jenvman.2020.111611

Kanchana P, Sekar C (2014) EDTA assisted synthesis of hydroxyapatite nanoparticles for electrochemical sensing of uric acid. Mater Sci Eng C 42:601–607. https://doi.org/10.1016/j.msec.2014.05.072

Koutsopoulos S (2002) Synthesis and characterization of hydroxyapatite crystals: a review study on the analytical methods. J Biomed Mater Res 62:600–612. https://doi.org/10.1002/jbm.10280

Lau OW, Ho SW (1993) Simultaneous determination of traces of iron, cobalt, nickel, copper, mercury and lead in water by energy-dispersive x-ray fluorescence spectrometry after preconcentration as their piperazino-1,4-bis(dithiocarbamate) complexes. Anal Chim Acta 280:269–277. https://doi.org/10.1016/0003-2670(93)85131-3

Leprêtre S, Chai F, Hildebrand JC, Martel B (2009) Prolonged local antibiotics delivery from hydroxyapatite functionalised with cyclodextrin polymers. Biomaterials 30:6086–6093. https://doi.org/10.1016/j.biomaterials.2009.07.045

Li Y, Liu X, Zeng X, Liu Y, Wei W, Luo S (2009) Simultaneous determination of ultra-trace lead and cadmium at a hydroxyapatite-modified carbon ionic liquid electrode by square-wave stripping voltammetry. Sensors Actuators B Chem 139:604–610. https://doi.org/10.1016/j.snb.2009.03.045

Li X, Zhou H, Fu C, Wang F, Ding Y, Kuang Y (2016) A novel design of engineered multi-walled carbon nanotubes material and its improved performance in simultaneous detection of Cd(II) and Pb(II) by square wave anodic stripping voltammetry. Sensors Actuators B Chem 236:144–152. https://doi.org/10.1016/j.snb.2016.05.149

Liu Q, de Wijn JR, de Groot K, van Blitterswijk CA (1998) Surface modification of nano-apatite by grafting organic polymer. Biomaterials 19:1067–1072. https://doi.org/10.1016/S0142-9612(98)00033-7

Liu Z, Xue Q, Guo Y (2017) Sensitive electrochemical detection of rutin and isoquercitrin based on SH-β-cyclodextrin functionalized graphene-palladium nanoparticles. Biosens Bioelectron 89:444–452. https://doi.org/10.1016/j.bios.2016.04.056

Longerich HP, Fryer BJ, Strong DF (1987) Determination of lead isotope ratios by inductively coupled plasma-mass spectrometry (ICP-MS). Spectrochim Acta Part B At Spectrosc 42:39–48. https://doi.org/10.1016/0584-8547(87)80048-4

Lv M, Wang X, Li J, Yang X, Zhang C, Yang J, Hu H (2013) Cyclodextrin-reduced graphene oxide hybrid nanosheets for the simultaneous determination of lead (II) and cadmium (II) using square wave anodic stripping voltammetry. Electrochim Acta 108:412–420. https://doi.org/10.1016/j.electacta.2013.06.099

Malode SJ, Shetti NP, Reddy KR (2021) Highly sensitive electrochemical assay for selective detection of aminotriazole based on $TiO_2$/poly (CTAB) modified sensor. Environ Technol Innov 21:101222. https://doi.org/10.1016/j.eti.2020.101222

Mobasherpour IL, Salahi E, Pazouki M (2011) Removal of divalent cadmium cations by means of synthetic nano crystallite hydroxyapatite. Desalination 266:142–148. https://doi.org/10.1016/j.desal.2010.08.016

Mohammadi S, Taher MA, Beitollahi H (2020) Synthesis and application of a natural-based nanocomposite with carbon nanotubes for sensitive voltammetric determination of lead (II) ions. Int J Environ Anal Chem 100:65–81. https://doi.org/10.1080/03067319.2019.1631300

Musa Y, Pudza ZZ, Abidin S, Abdul-Rashid F, Yasin ASM, Noor J, Abdullah (2020) Selective and simultaneous detection of cadmium lead and copper by tapioca-derived carbon dot–modified electrode. Environ Sci Pollut Res 27(12):13315–13324. https://doi.org/10.1007/s11356-020-07695-7

Nandi SK, Kundu B, Mukherjee J, Mahato A, Datta S, Balla VK (2015) Converted marine coral hydroxyapatite implants with growth factors: in vivo bone regeneration. Mater Sci Eng C 49:816–823. https://doi.org/10.1016/j.msec.2015.01.078

Ngassa GBP, Tonle IK, Walcarus A (2014) One-step co-intercalation of cetyltrimethylammonium and thiourea in smectite and application of the organoclay to the sensitive electrochemical detection of Pb(II). Appl Clay Sci 99:297–305. https://doi.org/10.1016/j.clay.2014.07.014

Niu X, Mo Z, Yang X, Sun M, Zhao P, Li Z, Ouyang M, Liu Z, Gao H, Guo R, Liu N (2018) Advances in the use of functional composites of β-cyclodextrin in electrochemical sensors. Microchim Acta 185:328–344. https://doi.org/10.1007/s00604-018-2859-6

Nouri-Felekori M, Khakbiz M, Nezafati N (2019) Synthesis and characterization of Mg, Zn and Sr-incorporated hydroxyapatite whiskers by hydrothermal method. Mater Lett 243:120–124. https://doi.org/10.1016/j.matlet.2019.01.147

Oliveira VHB, Rechotnek F, da Silva EP, Marques VS, Rubira AF, Silva R, Lourenco SA, Muniz EC (2020) A sensitive electrochemical sensor for $Pb^{2+}$ ions based on ZnO nanofibers functionalized by L-cysteine. J Mol Liq 309:113041. https://doi.org/10.1016/j.molliq.2020.113041

Othmani M, Aissa A, Bac CG, Rachdi F, Debbabi M (2013) Surface modification of calcium hydroxyapatite by grafting of etidronic acid. Appl Surf Sci 274:151–157. https://doi.org/10.1016/j.apsusc.2013.03.002

Pal A, Maity S, Chabri S, Bera S, Chowdhury AR, Das M, Sinha A (2017) Mechanochemical synthesis of nanocrystalline hydroxyapatite from mercenaria clam shells and phosphoric acid. Biomed Phys Eng Expr 3:015010. https://doi.org/10.1088/2057-1976/aa54f5

Pan W, Wang Y, Chen Z, Lou T, Qin W (2009) Nanomaterial/ionophore-based electrode for anodic stripping voltammetric determination of lead: an electrochemical sensing platform toward heavy metals. Anal Chem 81:5088–5094. https://doi.org/10.1021/ac900417e

Patel S, Han J, Qiu W, Gao W (2015) Synthesis and characterisation of mesoporous bone char obtained by pyrolysis of animal bones, for environmental application. J Environ Chem Eng 3:2368–2377. https://doi.org/10.1016/j.jece.2015.07.031

Prongmanee W, Alam I, Asanithi P (2019) Hydroxyapatite/Graphene oxide composite for electrochemical detection of L-Tryptophan. J Taiwan Inst Chem Eng 102:415–423. https://doi.org/10.1016/j.jtice.2019.06.004

Sadat-Shojai M, Khorasani MT, Dinpanah-Khoshdargi E, Jamshidi H (2013) Synthesis methods for nanosized hydroxyapatite with diverse structures. Acta Biomater 9:7591–7621. https://doi.org/10.1016/j.actbio.2013.04.012

Saoiabi S, EL Asri S, Laghzizil A, Coradin T, Lahlil K (2010) Nanoporous surface of organofunctionalized hydroxyapatite fabricated from natural phosphate rock. Mater Lett 64:2679–2681. https://doi.org/10.1016/j.matlet.2010.09.013

Shetti NP, Malode SJ, Nandibewoor ST (2015) Electro-oxidation of captopril at a gold electrode and its determination in pharmaceuticals and human fluids. Anal Methods 7(20):8673–8682. https://doi.org/10.1039/C5AY01619C

Shetti NP, Malode SJ, Malladi RS, Nargund SL, Shukla SS, Aminabhavi TM (2019) Electrochemical detection and degradation of textile dye Congo red at graphene oxide modified electrode. Microchem J 146:387–392. https://doi.org/10.1016/j.microc.2019.01.033

Sinha A, Mishra T, Ravishankar N (2008) Polymer assisted hydroxyapatite microspheres suitable for biomedical application. J Mater Sci Mater Med 19:2009–2013. https://doi.org/10.1007/s10856-007-3286-0

Sun M, Li Z, Wu S, Gu Y, Li Y (2018) Simultaneous detection of $Pb^{2+}$, $Cu^{2+}$ and $Hg^{2+}$ by differential pulse voltammetry at an indium tin oxide glass electrode modified by hydroxyapatite. Electrochim Acta 283:1223–1230. https://doi.org/10.1016/j.electacta.2018.07.019

Tang W, Zhao J, Sha B, Liu H (2013) Adsorption and drug release based on β-cyclodextrin-grafted hydroxyapatite composite. J Appl Polym Sci 127:2803–2808. https://doi.org/10.1002/app.37607

Tcheumi HL, Tassontio VN, Tonle IK, Ngameni E (2019) Surface functionalization of smectite-type clay by facile polymerization of β-cyclodextrin using citric acid cross linker: application as sensing material for the electrochemical determination of paraquat. Appl Clay Sci 173:97–106. https://doi.org/10.1016/j.clay.2019.03.013

Tchoffo R, Ngassa GBP, Tonle IK, Ngameni E (2021) Electroanalysis of diquat using a glassy carbon electrode modified with natural hydroxyapatite and β-cyclodextrin composite. Talanta 222:121550. https://doi.org/10.1016/j.talanta.2020.121550

Tonle IK, Ngameni E, Tchieno FMM, Walcarius A (2015) Organoclay-modified electrodes: preparation, characterization and recent electroanalytical applications. J Solid State Electrochem 19:1949–1973. https://doi.org/10.1007/s10008-014-2728-0

Tseng YH, Kuo CS, Li YY, Huang CP (2009) Polymer-assisted synthesis of hydroxyapatite nanoparticle. Mater Sci Eng C 29:819–822. https://doi.org/10.1016/j.msec.2008.07.028

Turk S, Altinsoy I, Efe G, Ipek M, Ozacar M, Bindal C (2019) Effect of Solution and Calcination Time on Sol-gel Synthesis of Hydroxyapatite. J Bionic Eng 16:311–318. https://doi.org/10.1007/s42235-019-0026-3

Xu T, Dai D, Jin Y (2020) Electrochemical sensing of lead (II) by differential pulse voltammetry using conductive polypyrrole nanoparticles. Microchim Acta 187:23–29. https://doi.org/10.1007/s00604-019-4027-z

Yala S, Khireddine H, Sidane D, Ziane S, Bir F (2013) Surface modification of natural and synthetic hydroxyapatites powders by grafting polypyrrole. J Mater Sci 48:7215–7223. https://doi.org/10.1007/s10853-013-7538-8

Yang L, Zhao H, Li CP, Fan S, Li B (2015) Dual β-cyclodextrin functionalized Au@SiC nanohybrids for the electrochemical determination of tadalafil in the presence of acetonitrile. Biosens Bioelectron 64:126–130. https://doi.org/10.1016/j.bios.2014.08.068

Yin H, Zhou Y, Ai S, Liu X, Zhu L, Lu L (2010) Electrochemical oxidative determination of 4-nitrophenol based on a glassy carbon electrode modified with a hydroxyapatite nanopowder. Microchim Acta 169:87–92. https://doi.org/10.1007/s00604-010-0309-1

Youness AR, Taha MA, Elhaes H, Ibrahim M (2017) Molecular modeling FTIR spectral characterization and mechanical properties of carbonated-hydroxyapatite prepared by mechanochemical synthesis. Mater Chem Phys 190:209–218. https://doi.org/10.1016/j.matchemphys.2017.01.004

Zhan F, Gao F, Wang X, Xie L, Gao F, Wang Q (2016) Determination of lead (II) by adsorptive stripping voltammetry using a glassy carbon electrode modified with β-cyclodextrin and chemically reduced graphene oxide composite. Microchim Acta 183:1169–1176. https://doi.org/10.1007/s00604-016-1754-2

Zhao HT, Ma S, Zheng SY, Han SW, Yao FX, Wang XZ, Wang SS, Feng K (2019) β–cyclodextrin functionalized biochars as novel sorbents for high-performance of $Pb^{2+}$ removal. J Hazard Mater 362: 206–213. https://doi.org/10.1016/j.jhazmat.2018.09.027

Zhu G, Yi Y, Chen J (2016) Recent advances for cyclodextrin-based materials in electrochemical sensing. Trends Anal Chem 80:232–241. https://doi.org/10.1016/j.trac.2016.03.022